Journal of the Physical Society of Japan
Vol. 73, No. 3, March, 2004, pp. 711–718

Resonant X-Ray Emission Spectroscopy in Scandium Halides

Masahiko MATSUBARA[1]*, Yoshihisa HARADA[2], Shik SHIN[1,2], Takayuki UOZUMI[3] and Akio KOTANI[2,4]

[1]*Institute for Solid State Physics, The University of Tokyo, 5-1-5, Kashiwanoha, Kashiwa, Chiba 277-8581*
[2]*RIKEN/SPring-8, 1-1-1, Mikazuki-cho, Sayo-gun, Hyogo 679-5148*
[3]*College of Engineering, Osaka Prefecture University, Sakai, Osaka 599-8531*
[4]*Photon Factory, IMSS, High Energy Accelerator Research Organization, Tsukuba, Ibaraki 305-0801*

(Received October 15, 2003)

Theoretical calculations of the Sc $2p \rightarrow 3d \rightarrow 2p$ resonant X-ray emission spectroscopy (RXES) in ScF_3, $ScCl_3$ and $ScBr_3$ are performed with a ScX_6 (X = F, Cl and Br) cluster model. Effects of intra-atomic multiplet coupling and interatomic hybridization are taken into account. The cluster model parameters for these materials are determined by analyzing experimental results of X-ray photoemission spectroscopy (XPS) and RXES. Some of the results are compared with new experimental data for $ScCl_3$ and $ScBr_3$. In the RXES results, we pay attention to the intensity ratio of the spectra arising from nonbonding states, which have mainly two peaks due to the crystal field splitting. From the change of the spectral intensity in RXES we find that the character of the highest energy structure of the main peaks in X-ray absorption spectroscopy (XAS) varies from almost pure e_g state to the e_g and t_{2g} mixed state depending on the strength of the multiplet effect and hybridization effect.

KEYWORDS: resonant X-ray emission, Sc halides, polarization dependence, cluster model, multiplet effect, hybridization effect
DOI: 10.1143/JPSJ.73.711

1. Introduction

Since the advent of high brightness synchrotron light sources, resonant X-ray emission spectroscopy (RXES) has been used as one of the useful tools to investigate electronic structures of transition metal compounds.[1–4] The RXES is a coherent second order optical process, where a core electron is excited to the threshold by an incident photon, and then the excited state decays by emitting an X-ray photon.[5,6] The intermediate state of RXES corresponds to the final state of X-ray absorption spectroscopy (XAS). Combining RXES with traditional techniques such as XAS and X-ray photoemission spectroscopy (XPS) enables us to study more detailed electronic states of subject materials.

The polarization dependence in RXES also provides us with more information about the electronic structure.[7–10] In previous papers,[8,9] we studied the $2p \rightarrow 3d \rightarrow 2p$ RXES of TiO_2 and ScF_3 ($3d^0$ systems) in "polarized" and "depolarized" configurations, and showed a drastic polarization dependence both theoretically and experimentally. The "polarized" configuration is the case where the polarization vector of the incident photon is perpendicular to the scattering plane, while the "depolarized" configuration is the case where it is parallel to the scattering plane. In both configurations the scattering angle is fixed to 90°, and the polarization of the emitted photon is not detected. More recently, we have extended the study to the $3d^1$, $3d^2$ and $3d^3$ systems: TiF_3, VF_3 and Cr_2O_3.[10]

In this paper we analyze, considering the polarization dependence, the RXES of ScF_3, $ScCl_3$ and $ScBr_3$, which are also classified into the $3d^0$ systems. For Sc compounds few systematic studies of electronic states with the change of ligand ions have so far been made. We analyze experimental results of XPS, XAS and RXES with a ScX_6 (X = F, Cl and Br) cluster model and determine the parameter values of the cluster model almost uniquely. In the $3d^0$ systems the RXES spectra have strong polarization dependence. The spectra obtained in the polarized configuration have mainly three structures: elastic scattering peak, strong inelastic scattering peak and weak inelastic scattering structure between the elastic and strong inelastic scattering peaks, whereas the spectra obtained in the depolarized configuration consist of only the weak inelastic scattering structure. In previous papers[9,10] we concentrate on the behavior of the elastic peak and the strong inelastic peak. But here we pay attention to the weak inelastic structure, which is mainly split into two peaks due to the crystal field energy, and its behavior of the relative intensity of these two peaks. From the analysis we find that the character of the highest energy peak of the main XAS peaks varies from the almost pure e_g state to the e_g and t_{2g} mixed state depending on the magnitude of the multiplet effect and hybridization effect.

In §2 we show the experimental results for $ScCl_3$ and $ScBr_3$, and then the model and formulation of theoretical calculations are given in §3. In §4 the calculated results are shown. Section 5 is devoted to the discussion.

2. Experimental Results

In this section we show the experimental results of Sc $2p$-XAS and RXES for $ScCl_3$ and $ScBr_3$. The $ScCl_3$ and $ScBr_3$ samples were prepared as pressed pellets of high purity (99.9%) powders. During the measurements, the samples were cooled down to 40 K and the base pressure of the experimental chamber was kept below 3×10^{-9} Torr.

The XAS results of $ScCl_3$ and $ScBr_3$ were obtained by the total photon yield (TPY) and total electron yield (TEY) methods, respectively. The RXES results were obtained using a Rowland mount type soft X-ray emission spectrometer system[11] installed at the undulator beamline BL-2C[12] of Photon Factory, KEK. The emission spectrometer has a laminar holographic grating whose radius and groove density are 5m and 1200 lines/mm. The polarization vector of the incident photon is linear and horizontal. The emission

*Present address: Institut de Physique et Chimie des Matériaux de Strasbourg, 23 rue du Loess, BP43 F-67034 Strasbourg Cedex 02, France.

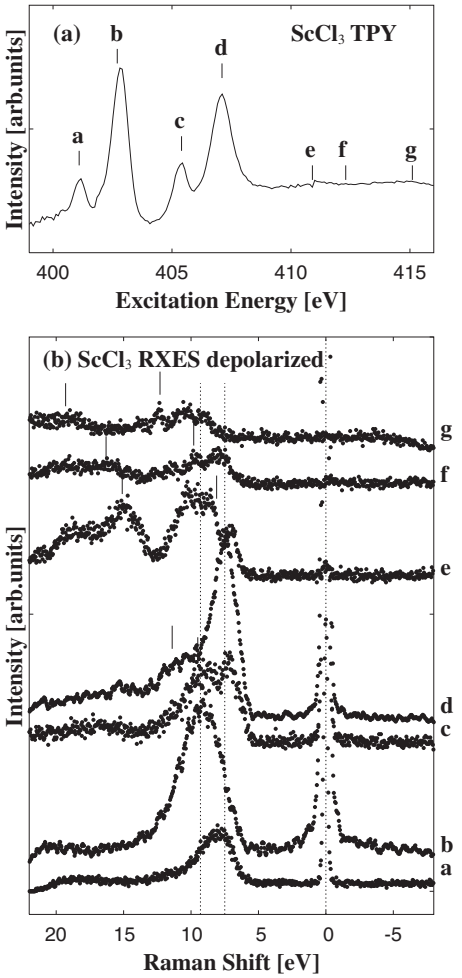

Fig. 1. Experimental results of (a) Sc $2p$ XAS and (b) Sc $2p \rightarrow 3d \rightarrow 2p$ RXES for $ScCl_3$. The RXES spectra are measured in the depolarized configuration. Indices **a** to **g** denote the incident photon energies.

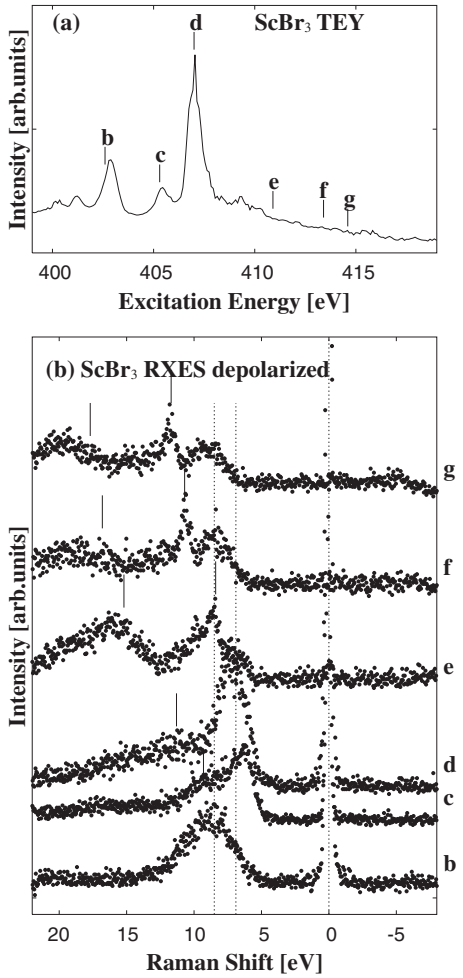

Fig. 2. Experimental results of (a) Sc $2p$ XAS and (b) Sc $2p \rightarrow 3d \rightarrow 2p$ RXES for $ScBr_3$. The RXES spectra are measured in the depolarized configuration. Indices **b** to **g** denote the incident photon energies.

spectrometer is mounted in a plane normal to the wave vector of the incident photon, which rotates 90° around the wave vector for polarization dependence of RXES. The incident angle of soft X-rays to the sample normal was 70° to reduce the self-absorption effect.

The energy resolution of the incident photon was about 0.2 eV at Sc $2p$ edge excitation. The total energy resolution of the RXES results was 0.6 eV at 400 eV using a 20 μm-wide incident slit of the spectrometer. The incident photon energy was calibrated by the photoemission of the gold $4f$ line. The emitted photon energy was calibrated using elastic scattering lines in the RXES results.

In Figs. 1 and 2 we show the results of (a) XAS and (b) RXES for $ScCl_3$ and $ScBr_3$, respectively. The XAS results show four main peaks and weak satellite structures similar to that of ScF_3,[13] although the energy difference between the main and satellite structures for $ScCl_3$ and $ScBr_3$ are smaller than that of ScF_3. The RXES result was obtained only in the depolarized configuration and plotted in the Raman shift representation. Vertical bars in each spectrum correspond to peak positions of a fluorescence spectrum which is not shown here.

3. Model and Formulation

In this section we first show the model Hamiltonian and spectral functions for XPS, XAS and RXES and then describe the way to determine the parameter values used in the present calculation.

3.1 Model and spectral functions

ScX_3 (X = F, Cl and Br) has slightly distorted octahedral structures around the Sc site.[14,15] We neglect this small distortion and assume that the local symmetry around the Sc ion is O_h. So the system under consideration is described by the ScX_6 cluster model.

The Hamiltonian consists of the Sc atomic part $H_{\rm Sc}$, the crystal field energy $H_{\rm CF}$, the p-molecular orbital energy $H_{\rm X}$ of ligand X and the mixing between the Sc $3d$ and X p states $H_{\rm mix}$:

$$H = H_{\rm Sc} + H_{\rm CF} + H_{\rm X} + H_{\rm mix}, \tag{1}$$

where

$$\begin{aligned} H_{\rm Sc} = &\sum_{\nu} \varepsilon_d d^\dagger_\nu d_\nu + \sum_{\mu} \varepsilon_p p^\dagger_\mu p_\mu + U_{dd} \sum_{\nu>\nu'} d^\dagger_\nu d_\nu d^\dagger_{\nu'} d_{\nu'} \\ &- U_{dc} \sum_{\nu,\mu} d^\dagger_\nu d_\nu (1 - p^\dagger_\mu p_\mu) + H_{\rm multiplet}, \end{aligned} \tag{2}$$

$$H_{\rm CF} = \sum_{\nu} \varepsilon(\Gamma) d^\dagger_\nu d_\nu,$$

$$\varepsilon(\Gamma) = \begin{cases} \dfrac{3}{5}(10Dq) & \text{if } \Gamma = e_g, \\ -\dfrac{2}{5}(10Dq) & \text{if } \Gamma = t_{2g}, \end{cases} \tag{3}$$

$$H_{\mathrm{X}} = \sum_{\nu} \varepsilon_{\mathrm{X}} X_{\nu}^{\dagger} X_{\nu}, \tag{4}$$

$$H_{\mathrm{mix}} = \sum_{\nu} V(\Gamma)(d_{\nu}^{\dagger} X_{\nu} + X_{\nu}^{\dagger} d_{\nu}). \tag{5}$$

Here $d_{\nu}^{\dagger}$ (d_{ν}), $p_{\mu}^{\dagger}$ (p_{μ}) and $X_{\nu}^{\dagger}$ (X_{ν}) are the electron creation (annihilation) operators for Sc $3d$, Sc $2p$ core orbitals and X p molecular orbitals, respectively. The indices ν and μ represent the spin (σ) and orbital (Γ) states, and Γ runs over t_{2g} and e_g, which are irreducible representations of O_h.

In eq. (2), ε_d and ε_p denote the one particle energies for Sc $3d$ and Sc $2p$ states, respectively, U_{dd} and U_{dc} describe the Coulomb interaction between Sc $3d$ electrons and the attracting core-hole potential acting on the $3d$ electrons, respectively, and the last term, $H_{\mathrm{multiplet}}$, consists of the multipole part of the Coulomb interaction and the spin–orbit interaction. In eqs. (3)–(5), $10Dq$ [$= \varepsilon(e_g) - \varepsilon(t_{2g})$], ε_{X} and $V(\Gamma)$ denote the crystal field splitting energy, one particle energy for X p state and hybridization between Sc $3d$ and X p states, respectively.

The charge transfer (CT) energy is defined as $\Delta = E(d^1\underline{X}) - E(d^0)$, where $\underline{X}$ denotes a hole in the X p orbital and $E(d^1\underline{X})$ and $E(d^0)$ are the configuration averaged energies of $d^1\underline{X}$ and d^0 configurations, respectively. We treat the Δ, U_{dd}, U_{dc}, $V(e_g)$ [$= -2V(t_{2g})$,[16,17] for simplicity], and $10Dq$ as adjustable parameters.

The Slater integrals, F^k and G^k, and the spin–orbit coupling constants, ζ_d and ζ_p, are calculated with an atomic Hartree–Fock calculation program and then the values of the Slater integrals are scaled down to those of 85% in order to empirically include the effect of intra-atomic configuration interaction from higher basis configurations which are not included in our calculation.

The XPS spectrum is expressed as

$$F_{\mathrm{XPS}}(E_{\mathrm{B}}) = \sum_{m'} \left|\langle m'|T_{\mathrm{i}}|g\rangle\right|^2 \delta(E_{\mathrm{B}} + E_g - E_{m'}). \tag{6}$$

In eq. (6), E_{B} denotes the binding energy, and $|g\rangle$, which is a linear combination of d^0, $d^1\underline{X}$ and $d^2\underline{X}^2$ configurations, represents the ground state of XPS with energy E_g. Also, $|m'\rangle$, which is a linear combination of $\underline{2p}d^0$, $\underline{2p}d^1\underline{X}$ and $\underline{2p}d^2\underline{X}^2$ configurations, represents the final state of XPS with energy $E_{m'}$. The electric dipole transition operator for an incident photon is given by T_{i}.

The XAS spectrum is written as

$$F_{\mathrm{XAS}}(\Omega) = \sum_{m} \left|\langle m|T_{\mathrm{i}}|g\rangle\right|^2 \delta(\Omega + E_g - E_m). \tag{7}$$

In eq. (7), Ω denotes the incident photon energy, and $|m\rangle$, which is a linear combination of $\underline{2p}d^1$, $\underline{2p}d^2\underline{X}$ and $\underline{2p}d^3\underline{X}^2$ configurations, denotes the final state of XAS with energy E_m.

The RXES spectrum is represented as

$$F(\Omega,\omega) = \sum_{f} \left| \sum_{m} \frac{\langle f|T_{\mathrm{e}}|m\rangle\langle m|T_{\mathrm{i}}|g\rangle}{E_m - E_g - \Omega - \mathrm{i}\Gamma_{\mathrm{L}}} \right|^2 \times \delta(\Omega - \omega + E_g - E_f). \tag{8}$$

In eq. (8), ω denotes the emitted photon energy, and $|f\rangle$, which is described by a linear combination of d^0, $d^1\underline{X}$ and $d^2\underline{X}^2$ configurations, represents the final state of RXES with energy E_f. The intermediate state $|m\rangle$ is the same as the final state of XAS, whose lifetime width is represented by Γ_{L}. The electric dipole transition operator for an emitted photon is given by T_{e}.

In order to consider the incident photon polarization, we convert eq. (8) into an appropriate form.[9,10] In our calculation, for simplicity, the direction of the incident photon propagation is assumed to be parallel to one of the cube axis, because the spectral shape of RXES is not practically affected by the incident photon direction under the O_h symmetry and 90° scattering angle situation. We eventually acquire the following spectral function of RXES for the polarized and depolarized configurations:

$$\begin{aligned} F(\Omega,\omega) &= \sum_{q,q'=\pm1} \sum_{f} \left| \sum_{m} \frac{\langle f|C_q^{(1)}|m\rangle\langle m|C_{q'}^{(1)}|g\rangle}{E_m - E_g - \Omega - \mathrm{i}\Gamma_{\mathrm{L}}} \right|^2 \\ &\quad \times \delta(\Omega - \omega + E_g - E_f) \\ &\quad \text{(polarized configuration)}, \\ F(\Omega,\omega) &= \sum_{q=\pm1} \sum_{f} \left| \sum_{m} \frac{\langle f|C_q^{(1)}|m\rangle\langle m|C_0^{(1)}|g\rangle}{E_m - E_g - \Omega - \mathrm{i}\Gamma_{\mathrm{L}}} \right|^2 \\ &\quad \times \delta(\Omega - \omega + E_g - E_f) \\ &\quad \text{(depolarized configuration)}. \end{aligned} \tag{9}$$

The XPS and XAS spectra are convoluted with both Lorentzian and Gaussian functions, whereas the RXES is convoluted only with a Gaussian function. The HWHM of the Lorentzian for XPS and XAS are $\Gamma_{\mathrm{L}} = 0.1\,\mathrm{eV}$. The HWHM of the Gaussian for XPS is $\Gamma_{\mathrm{G}} = 0.7\,\mathrm{eV}$, whereas the HWHM for XAS and RXES are $\Gamma_{\mathrm{G}} = 0.5\,\mathrm{eV}$.

3.2 Parameter values

As mentioned above, the adjustable parameters used in the present calculation are Δ, U_{dd}, U_{dc}, $V(e_g)$ and $10Dq$. In addition, we take the scaling factors of configuration dependent hybridization, R_c and R_v, into account.[18–21] Due to the core-hole creation, the wave function of $3d$ states is contracted in the core excited state and the hybridization strength becomes smaller. The scaling factor of this effect is denoted by R_c. On the other hand, when the electron number increases, the wave function is spatially extended and the hybridization strength becomes larger. The factor of this effect is denoted by R_v. The relationship between the electronic configurations and these factors are illustrated in Fig. 3.

So far, Sc compounds are hardly dealt with by the cluster model or impurity Anderson model and their parameter values are not well established. Therefore we start from determining those parameter values. For simplicity, we fix some parameter values as $10Dq = 1.0$ eV, $R_c = 0.9$ and $R_v = 0.9$ and also assume the relation $U_{dd} = 0.7U_{dc}$. The procedure to estimate Δ, U_{dc} and $V(e_g)$ are briefly described in the following paragraph.

We know the experimental values of the energy difference (dE_{B}) between the $2p_{3/2}$ main peak and the satellite and the

Table I. Parameter values used in the calculation, which are given in units of eV except for R_c and R_v. The energy difference dE_B (eV) and the intensity ratio I_s/I_m between the $2p_{3/2}$ main peak and the satellite of Sc $2p$-XPS, and the energy difference dE_{nb} (eV) between the elastic peak and the center of gravity of the inelastic structures of Sc $2p \rightarrow 3d \rightarrow 2p$ RXES obtained from the calculated (experimental) results are also included.

Compounds	Δ	U_{dd}	U_{dc}	$V(e_g)$	$10Dq$	R_c	R_v	dE_B	I_s/I_m	dE_{nb}
ScF_3	11.5	7.7	11.0	3.2	1.0	0.9	0.9	12.2 (12.3)	0.28 (0.25)	13.6 (13.6)
$ScCl_3$	6.0	4.6	6.5	2.5	1.0	0.9	0.9	9.6 (9.6)	0.21 (0.2)	8.4 (8.4)
$ScBr_3$	5.5	3.5	5.0	2.3	1.0	0.9	0.9	8.5 (8.6)	0.15 (0.15)	7.7 (7.7)

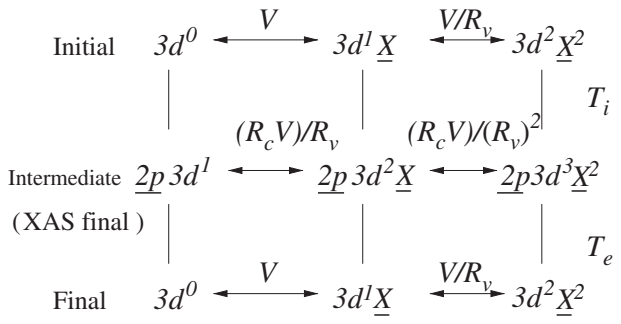

Fig. 3. Relationship between the scaling factors R_c and R_v and the hybridization strength V in the $3d^0$ system.

intensity ratio (I_s/I_m) of the satellite (I_s) to main peak (I_m) from the XPS results. Also, we know the experimental value of the energy difference (dE_{nb}) between the elastic peak and the center of gravity of the inelastic structures from the RXES results obtained in the depolarized configuration. By our cluster model calculation we plot the U_{dc}/V_{eff} as a function of Δ/V_{eff}, where V_{eff} denotes the effective hybridization defined by

$$V_{eff} = \sqrt{6V(t_{2g})^2 + 4V(e_g)^2}, \\ = \sqrt{\frac{11}{2}}V(e_g), \tag{10}$$

with keeping the dE_B, I_s/I_m and dE_{nb} as the experimental values. The case for $ScBr_3$ is shown, as an example, in Fig. 4. When three curves of dE_B, I_s/I_m and dE_{nb} cross at one point, the three conditions to reproduce the three experimental values are fulfilled, and thus the parameter values are determined uniquely. In the $ScBr_3$ case, when $V_{eff} = 4.85$, the three curves almost cross at one point. Therefore, we find that the parameter values of Δ, U_{dc} and $V(e_g)$ for $ScBr_3$ are 5.5 eV, 5.0 eV and 2.3 eV, respectively.

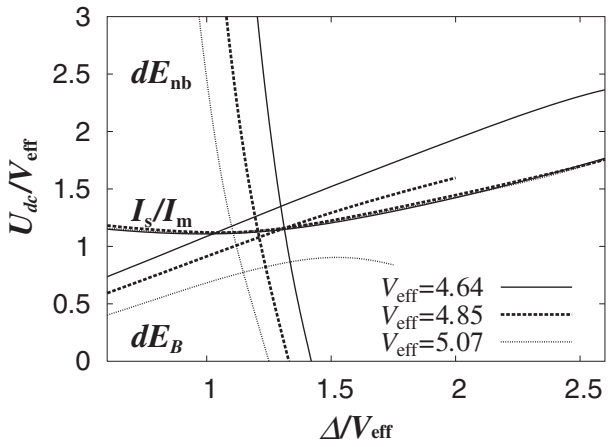

Fig. 4. Theoretical curves for $ScBr_3$ which keep dE_B, I_s/I_m and dE_{nb} constant. The parameter values U_{dc} and Δ are in units of V_{eff} which are 4.64, 4.85 and 5.07.

The same procedures are performed for ScF_3 and $ScCl_3$ and we obtain the parameter values shown in Table I. The parameter values for $ScCl_3$ and $ScBr_3$ are newly determined in this paper, whereas those for ScF_3 are somewhat different from those in ref. 9. This is because with old parameter values of ScF_3 the experimental results of XAS and RXES are reproduced well, but we find that those of XPS cannot be reproduced (the calculated satellite intensity is much smaller than the experimental one). As shown in the next section, we can successfully reproduce all the experimental results of XPS, XAS and RXES with new ones shown in Table I.

4. Calculated Results of XPS, XAS and RXES

In this section we show the calculated results of Sc $2p$-XPS, $2p$-XAS and $2p \rightarrow 3d \rightarrow 2p$ RXES for ScX_3 (X = F, Cl and Br). The parameter values, which are estimated by the procedure described in the preceding section, are used in the calculation.

4.1 Sc 2p-XPS

First of all we show the calculated results of Sc $2p$-XPS for ScX_3 (X = F, Cl and Br) in Fig. 5(b), which are in good agreement with the experimental results by de Boer *et al.*[22] shown in Fig. 5(a). All the spectra consist of four peaks and they are assigned to $2p_{3/2}$ main, $2p_{1/2}$ main, $2p_{3/2}$ satellite and $2p_{1/2}$ satellite peaks from low to high energies, respectively. We can see that the energy difference between the main peak and the satellite, dE_B, becomes smaller and the intensity ratio, I_s/I_m, also becomes smaller as the ligand changes from F to Br. These values are also summarized in Table I.

4.2 Sc 2p-XAS and Sc 2p → 3d → 2p RXES

Here we show the calculated results of Sc $2p$-XAS and Sc $2p \rightarrow 3d \rightarrow 2p$ RXES for ScX_3 (X = F, Cl and Br).

In Fig. 6, the experimental [(a) and (b)] and calculated [(c) and (d)] results of Sc $2p$-XAS and Sc $2p \rightarrow 3d \rightarrow 2p$ RXES for ScF_3 are shown. The experimental result of Sc $2p$-XAS was obtained by Umeda *et al.*[13] and that of Sc $2p \rightarrow 3d \rightarrow 2p$ RXES is reproduced from ref. 9. In Figs. 7 and 8, the calculated results of (a) Sc $2p$-XAS and (b) Sc $2p \rightarrow 3d \rightarrow 2p$ RXES for $ScCl_3$ and $ScBr_3$, respectively, are shown. All the Sc $2p$-XAS spectra mainly consist of four peaks due to the crystal field (for $3d$ states) and the spin–orbit splitting (for $2p$ states). Furthermore, the weak satellite structure is seen on the higher energy side of the main peaks. We also show a 20 times magnified spectrum around the satellite structure. Indices **a**, **b**, ..., etc. in Figs. 6–8 denote the

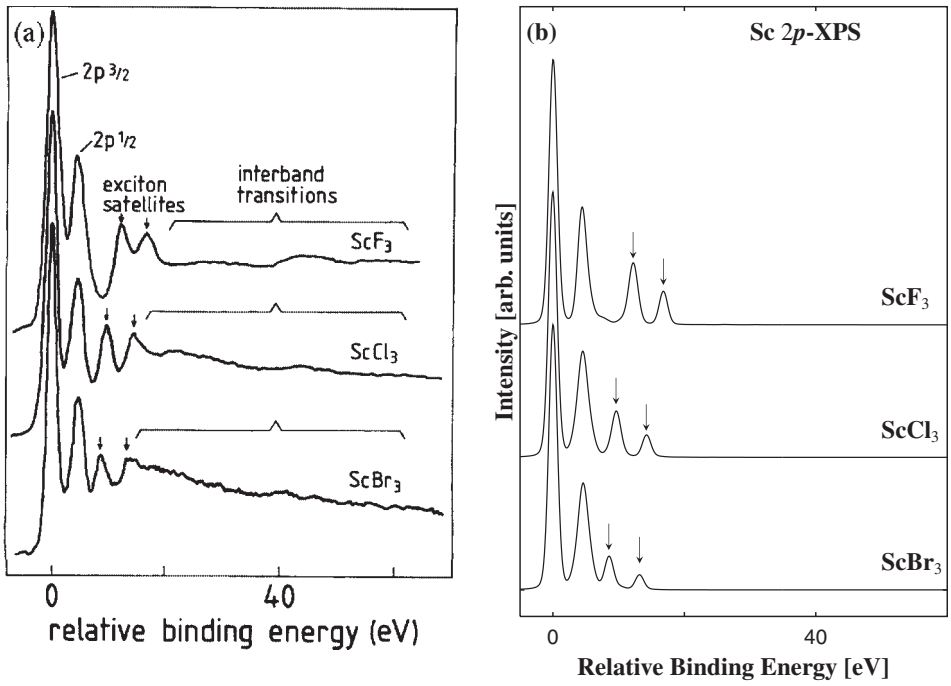

Fig. 5. (a) Experimental[22] and (b) calculated results of Sc $2p$-XPS for ScX_3 (X = F, Cl and Br). All the spectra consist mainly of four peaks and the main peaks of $2p_{3/2}$ are set to 0 eV. Satellite peaks are indicated by arrows.

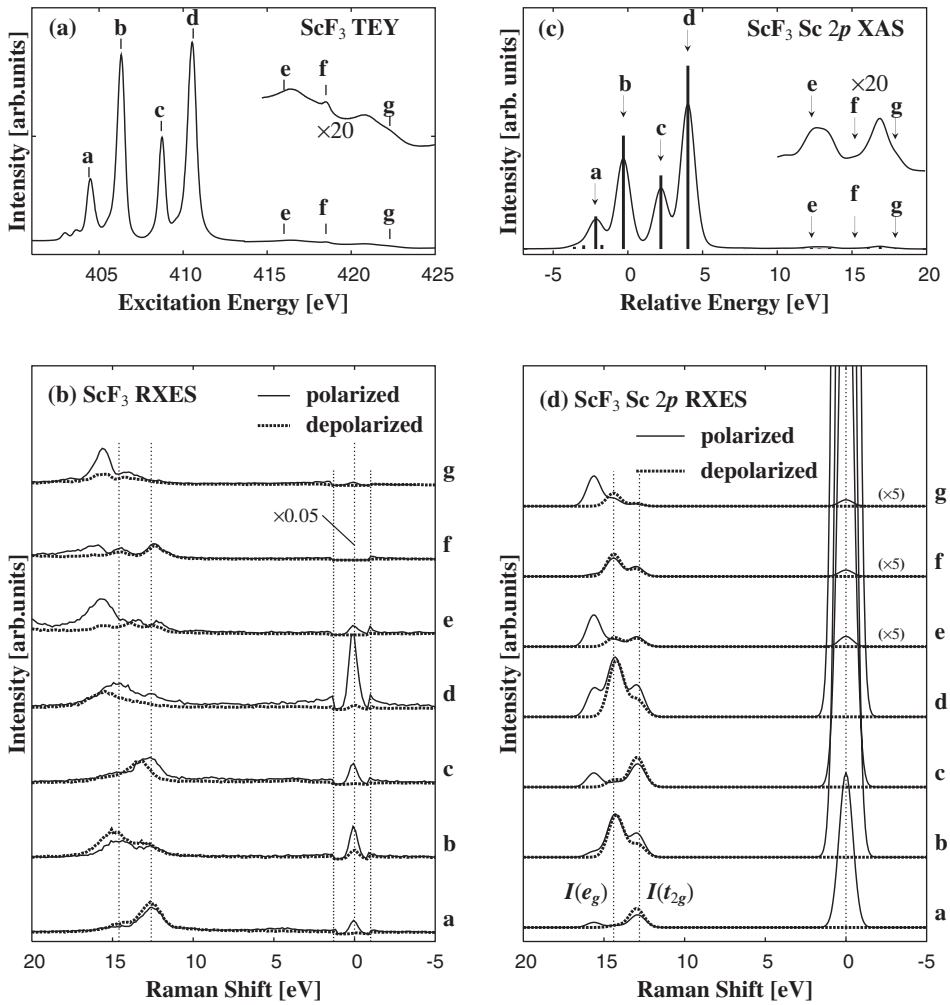

Fig. 6. Experimental results of (a) Sc $2p$-XAS and (b) Sc $2p \rightarrow 3d \rightarrow 2p$ RXES[13] and the calculated results of (c) Sc $2p$-XAS and (d) Sc $2p \rightarrow 3d \rightarrow 2p$ RXES for ScF_3. The RXES spectra in the polarized configuration are plotted with solid lines, while those in the depolarized configuration with dashed lines. Indices from **a** to **g** denote the incident photon energies. In XAS the satellite region is magnified by a factor of 20. In RXES the spectra from **e** to **g** are enlarged by a factor of 5. In the experimental result of RXES, the elastic peak is suppressed by a factor of 1/20.

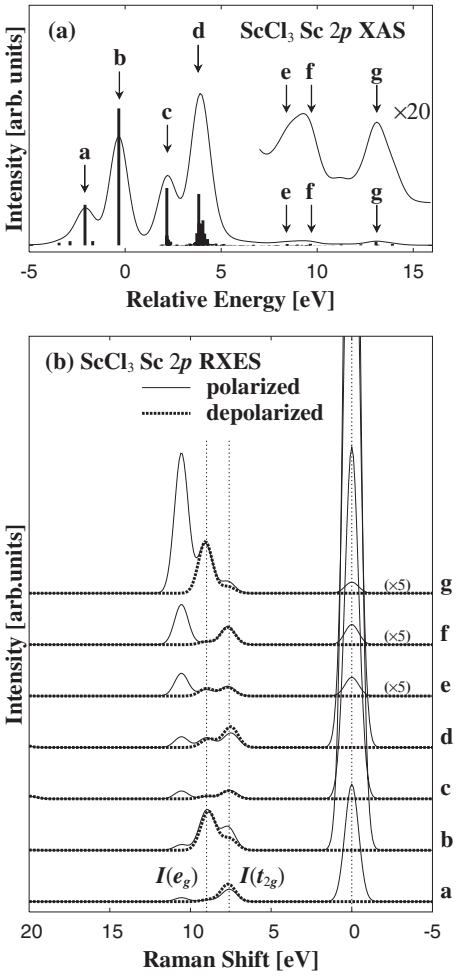

Fig. 7. Calculated results of (a) Sc $2p$ XAS and (b) Sc $2p \rightarrow 3d \rightarrow 2p$ RXES for $ScCl_3$. In XAS the satellite regions is magnified by a factor of 20. In RXES, spectra in the polarized configuration are plotted with solid lines, while those in the depolarized configuration with dashed lines. Indices from **a** to **g** denote the incident photon energies. In RXES spectra from **e** to **g** are enlarged by a factor of 5.

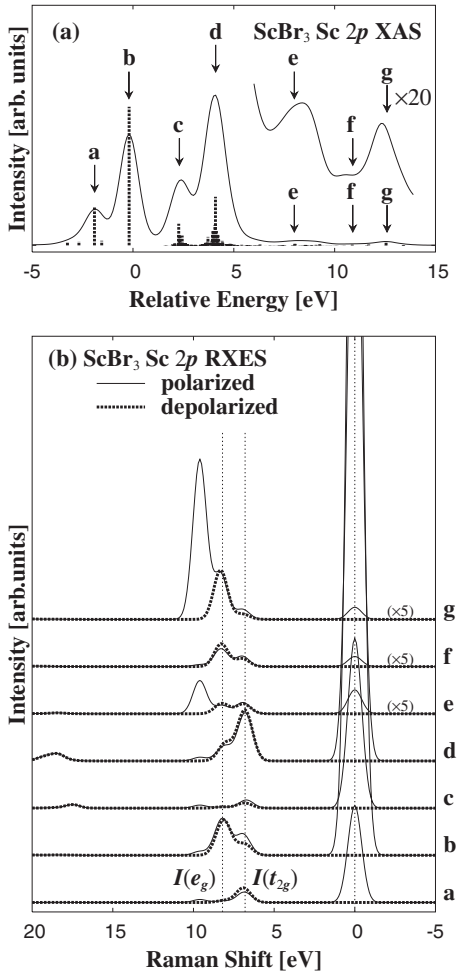

Fig. 8. Calculated results of (a) Sc $2p$-XAS and (b) Sc $2p \rightarrow 3d \rightarrow 2p$ RXES for $ScBr_3$. In XAS the satellite region is magnified by a factor of 20. In RXES, spectra in the polarized configuration are plotted with solid lines, while those in the depolarized configuration with dashed lines. Indices from **b** to **g** denote the incident photon energies. In RXES spectra from **e** to **g** are enlarged by a factor of 5.

incident photon energies of RXES.

In the experimental results of $ScCl_3$ [Fig. 1(b)] and $ScBr_3$ [Fig. 2(b)], the spectra shifting to the lower energy side whose energy shift is proportional to the incident photon energy are seen. This means that the emitted photon energy is nearly independent of the incident photon energy as in the case of normal XES (NXES). These so-called "NXES-like spectra" are not seen in the calculated results. Since this kind of spectra results from multi-transition-metal-site effect,[23] we cannot reproduce such structures within the model used in this paper. Except for these NXES-like spectra, however, agreement between the calculated and experimental results is fairly good.

All the Sc $2p \rightarrow 3d \rightarrow 2p$ RXES spectra are plotted as functions of Raman shift energy. The indices denote the incident photon energies, which correspond to those written in the XAS results. All the calculated results are obtained both in the polarized and depolarized configurations, although the experimental results for $ScCl_3$ and $ScBr_3$ are obtained only in the depolarized configuration.

The spectra obtained in the polarized configuration are plotted with solid lines, where an elastic peak at 0 eV is enhanced when the incident photon energy is set to the main peak energy of XAS, and an inelastic peak, which appears at the highest Raman shift energy, is enhanced when the incident photon energy is set to the satellite energy of XAS. On the other hand, the spectra obtained in the depolarized configurations are plotted with dashed lines, where we have no enhancement for both the elastic and highest energy inelastic peaks. The other inelastic features than the highest energy inelastic peak appear both in the polarized and depolarized configurations and are split into two peaks due to the crystal-field splitting. In the following, we call the higher energy peak $I(e_g)$ and the lower one $I(t_{2g})$.

In ScF_3, $I(t_{2g})$ is enhanced when the incident photon energy is set to the t_{2g} peaks of XAS (**a** and **c**), while $I(e_g)$ is enhanced when the incident photon energy is set to the e_g peaks of XAS (**b** and **d**). These spectral features are in good agreement with experimental result [Fig. 6(b)]. In the meantime, in $ScCl_3$ and $ScBr_3$ when the incident photon energy is set to the t_{2g} peaks of XAS (**a**, only for $ScCl_3$, and **c**), $I(t_{2g})$ is enhanced. When the incident photon energy is set to **b**, $I(e_g)$ is enhanced, in the same manner as ScF_3, but when the incident photon energy is set to **d**, $I(t_{2g})$ is enhanced contrary to the case of ScF_3. This spectral behavior is also seen in the experimental results for $ScCl_3$

and $ScBr_3$.

We find here, both from the experimental and theoretical studies, quite interesting facts: (1) the e_g excitation leads to the t_{2g} enhancement, (2) this occurs only in $2p_{1/2}$ branch, and (3) this is not seen in ScF_3 but seen in $ScCl_3$ and $ScBr_3$. In the next section we will discuss what causes these strange spectral behaviors in detail.

5. Discussion

The mechanism of RXES is well described by the schematic total energy-level diagram shown in Fig. 9. The RXES spectra obtained in the polarized configuration mainly consist of three parts. They correspond to the bonding, nonbonding and antibonding states, respectively. The bonding and antibonding states originate from strongly hybridized $3d^0$ and $3d^1\underline{X}$ states, while the nonbonding state originates from other unhybridized states. In the case of ScF_3, for example, the elastic peak corresponds to the bonding state, the $\sim$13 eV and $\sim$15 eV inelastic peaks to the nonbonding states and the $\sim$16 eV inelastic peak to the antibonding state.

In the $3d^0$ system, whose ground state symmetry is A_{1g}, only the inelastic structure arising from nonbonding state appears in the depolarized configuration due to the selection rule.[9)]

In Table II, we display the energy difference between these inelastic peaks and the elastic peak both in the experimental and calculated results of Sc $2p \rightarrow 3d \rightarrow 2p$ RXES. The values obtained from calculations are in good agreement with those from experiments. Moreover, as shown in Table I, we almost reproduce the energy difference and intensity ratio between the main peak and the satellite in Sc $2p$-XPS. The parameter values used in this calculation are selected to reproduce the Sc $2p$-XPS, $2p$-XAS and $2p \rightarrow 3d \rightarrow 2p$ RXES simultaneously, so that we can expect they reflect the electronic structure of each compound very well.

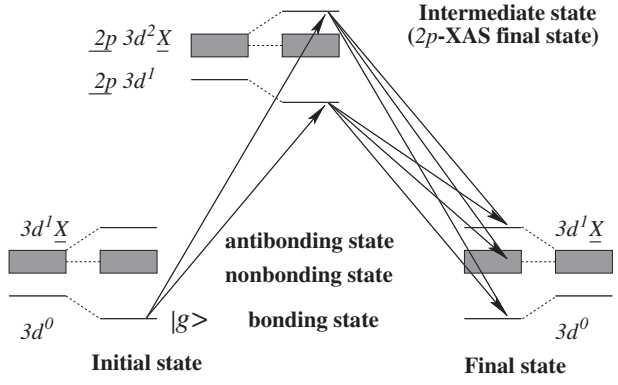

Fig. 9. Schematic total energy-level diagram of $2p \rightarrow 3d \rightarrow 2p$ RXES for $3d^0$ system.[9)] Only the lowest two configurations are considered and the crystal field and spin–orbit splittings are neglected for simplicity.

From Table I we notice that the parameter values for the CT energy Δ and the core-hole potential U_{dc} largely change on going from F to Br. As for the CT energy, it is well known that the change of the ligand leads to the change of the electro-negativity of ligand X and thereby the value of the CT energy varies. The magnitude of the electro-negativity decreases from F to Br: F > Cl > Br. The larger the electro-negativity is, the more difficult the CT from ligand p to Sc $3d$ states is, so that Δ becomes larger.

On the other hand, as for the d–d Coulomb interaction, U_{dd}, and the core-hole potential, U_{dc}, the values are considered to be almost independent of ligand ions as long as the metal ion is unchanged. In fact, in the analyses of the various core level spectroscopy of late transition-metal compounds, U_{dd} and U_{dc} have almost the same values if the metal ion is the same.[24–26)] In the case of Sc compounds, however, it is difficult to reproduce the experimental results if we keep the value of U_{dc} constant. According to de Boer *et al.*[22)] the core-hole potential is written as follows:

$$U_{dc} = Q_0 - 2E_p \tag{11}$$

where Q_0 denotes the Coulomb interaction between the core-hole and the $3d$ electron and E_p denote the polarization energy. This inconsistency on U_{dc} between the early and late transition metal compounds may suggest that the influence of E_p on U_{dc} in the former is different from that in the latter. However, the detailed microscopic mechanism is still unclear, and remains as a future problem.

The reason why $I(t_{2g})$ is enhanced when the incident photon energy is set to the t_{2g} peaks of XAS, whereas $I(e_g)$ is enhanced when the incident photon energy is set to the e_g peaks of XAS for ScF_3 is explained by the simple one-electron picture. When the $2p$ electron is excited to the $3d$ states, whose symmetry is t_{2g}, the electronic configuration in the intermediate state of RXES (the final state of XAS) is written as $\underline{2p}3d^1(t_{2g})$, where $\underline{2p}$ denotes a $2p$ core-hole. This is mixed with the ligand orbitals through the hybridization, so $\underline{2p}3d^2(t_{2g}e_g)\underline{X}(e_g)$ and $\underline{2p}3d^2(t_{2g}t_{2g})\underline{X}(t_{2g})$ can exist. In the decay process, a $3d$ electron fills the core-hole. From $\underline{2p}3d^2(t_{2g}t_{2g})\underline{X}(t_{2g})$ only $3d^1(t_{2g})\underline{X}(t_{2g})$ can be reached, whereas from $\underline{2p}3d^2(t_{2g}e_g)\underline{X}(e_g)$ either $3d^1(t_{2g})\underline{X}(e_g)$ or $3d^1(e_g)\underline{X}(e_g)$ can be reached. In the $3d^1(t_{2g})\underline{X}(t_{2g})$ and $3d^1(e_g)\underline{X}(e_g)$ configurations, the Sc $3d$ electron and the ligand hole have the same symmetry, so that they are strongly hybridized and assigned to the bonding and antibonding states, while in the $3d^1(t_{2g})\underline{X}(e_g)$ configuration the Sc $3d$ and $\underline{X}$ states do not have the same symmetry, so that they are not hybridized at all and are assigned to the nonbonding state and the symmetry of $3d$ electron is t_{2g},

Table II. Energy difference between the $I(t_{2g})$ [$I(e_g)$] and the the elastic peak of RXES, which are denoted as $dE_{nb}(1)$ [$dE_{nb}(2)$], and that between the inelastic spectrum arising from the antibonding state and the elastic peak of RXES, which is denoted as dE_{ab}. Both experimental and calculated results are shown. Unknown values are displayed by horizontal bars.

Compounds	Experiment			Calculation		
	$dE_{nb}(1)$	$dE_{nb}(2)$	dE_{ab}	$dE_{nb}(1)$	$dE_{nb}(2)$	dE_{ab}
ScF_3	12.6	14.6	15.7	12.8	14.4	15.6
$ScCl_3$	7.5	9.3	—	7.6	9.0	10.5
$ScBr_3$	6.9	8.5	—	6.8	8.2	9.6

which leads to the enhancement of $I(t_{2g})$.

In the case of e_g, the same process occurs. In the intermediate state $\underline{2p}3d^1(e_g)$, its charge transfer states from the ligand to the metal ion, $\underline{2p}3d^2(e_g t_{2g})\underline{X}(t_{2g})$ and $\underline{2p}3d^2(e_g e_g)\underline{X}(e_g)$ exist. After the decay process, the non-bonding state has the $3d^1(e_g)\underline{X}(t_{2g})$ configuration and $I(e_g)$ is enhanced.

As mentioned in the preceding section, in ScF_3 when the incident photon energy is set to the XAS peaks of t_{2g} symmetry (**a** and **c**), $I(t_{2g})$ is enhanced, and when the incident photon energy is set to the XAS peaks of e_g (**b** and **d**), $I(e_g)$ is enhanced. This is consistent with the above mentioned simple one-electron picture. In the cases of $ScBr_3$ and $ScCl_3$, however, the situation is somewhat different. When the incident photon energy is set to **a**, **b** and **c**, the enhancement behavior is the same as in the case of ScF_3. However, when the incident photon energy is set to **d**, the enhanced peak is not $I(e_g)$ but $I(t_{2g})$.

The reversal of intensity in $ScCl_3$ and $ScBr_3$ is caused by the deviation from the above-mentioned one-electron picture due to the strong multiplet coupling and strong hybridization effects. In order to show this, we have calculated the intensity ratio $I(e_g)/I(t_{2g})$ at the resonance **d** with the parameters for $ScCl_3$ but by changing the scaling factor for the Slater integrals (denoted as *multiplet scaling factor*). The result is shown in Fig. 10 with the solid curve. It is seen that if the multiplet coupling is weak enough we have the normal result $I(e_g)/I(t_{2g}) > 1.0$. When the multiplet scaling factor is larger than 0.5, the reversal of intensity occurs, so that for $ScCl_3$ (scaling factor of 0.85) we have $I(e_g)/I(t_{2g}) < 1.0$. This is because the simple one electron picture breaks down, and the e_g and t_{2g} electronic states are mixed strongly, by the strong multiplet coupling effect. This multiplet effect has strong influence on XAS spectra around **d** but it becomes weaker in going to lower energy as seen from the line spectra in Figs. 7(a) and 8(a); the line spectra are split into many lines for **d**, but it is not the case for **a**, **b** and **c**. This is why the reversal does not occur at resonance **a**, **b** and **c** but occur at **d**.

We have made a similar calculation with $\Delta = 12.0\,\mathrm{eV}$ (instead of 6.0 eV), and obtained the result shown with the dashed curve in Fig. 10. Now we find that the reversal of intensity occurs for the multiplet scaling factor larger than 1.2. This is because the deviation from the one-electron picture is suppressed due to the weaker hybridization effect (i.e. the effect of the larger Δ), and explains why the reversal of intensity disappears for ScF_3. Note that the line spectra of Fig. 6(c) do not split into many lines even for **d**.

We can directly observe the breakdown of the one-electron picture from the RXES results and these results also suggest that the peak **d** of XAS for $ScCl_3$ and $ScBr_3$ is not almost pure e_g state, but t_{2g} and e_g mixed state.

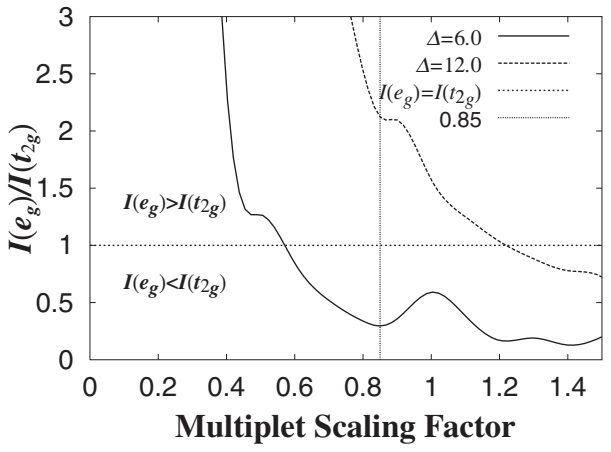

Fig. 10. $I(e_g)/I(t_{2g})$ when the multiplet coupling of the intermediate state is scaled from 0 to 1.5.

Acknowledgments

This work is partially supported by a Grant-in-Aid for JSPS Fellows from the Ministry of Education, Culture, Sports, Science and Technology. One of the authors (M.M.) is financially supported by JSPS Research Fellowships for Young Scientists. The finish of this paper has been made when M.M. stays at IPCMS in Strasbourg, and he would like to thank Dr. J.-C. Parlebas for his hospitality and for valuable discussion on this work.

1) C.-C. Kao, W. A. L. Caliebe, J. B. Hastings and J.-M. Gillet: Phys. Rev. B **54** (1996) 16361.
2) J. P. Hill, C.-C. Kao, W. A. L. Caliebe, M. Matsubara, A. Kotani, J. L. Peng and R. L. Greene: Phys. Rev. Lett. **80** (1998) 4967.
3) J. Jiménez-Mier, J. van Ek, D. L. Ederer, T. A. Callcott, J. J. Jia, J. Carlisle, L. Terminello, A. Asfaw and R. C. Perera: Phys. Rev. B **59** (1999) 2649.
4) H. Ishii, Y. Ishiwata, R. Eguchi, Y. Harada, M. Watanabe, A. Chainani and S. Shin: J. Phys. Soc. Jpn. **70** (2001) 1813.
5) S. Tanaka, K. Okada and A. Kotani: J. Phys. Soc. Jpn. **60** (1991) 3893.
6) A. Kotani and S. Shin: Rev. Mod. Phys. **73** (2001) 203.
7) L. C. Duda, G. Dräger, S. Tanaka, A. Kotani, J. Guo, D. Heumann, S. Bocharov, N. Wassdahl and J. Nordgren: J. Phys. Soc. Jpn. **67** (1998) 416.
8) Y. Harada, T. Kinugasa, R. Eguchi, M. Matsubara, A. Kotani, M. Watanabe, A. Yagishita and S. Shin: Phys. Rev. B **61** (2000) 12854.
9) M. Matsubara, T. Uozumi, A. Kotani, Y. Harada and S. Shin: J. Phys. Soc. Jpn. **69** (2000) 1558.
10) M. Matsubara, T. Uozumi, A. Kotani, Y. Harada and S. Shin: J. Phys. Soc. Jpn. **71** (2002) 347.
11) Y. Harada, H. Ishii, M. Fujisawa, Y. Tezuka, S. Shin, M. Watanabe, Y. Kitajima and A. Yagishita: J. Synchrotron Radiat. **5** (1998) 1013.
12) M. Watanabe, A. Toyoshima, Y. Azuma, T. Hayaishi, Y. Yan and A. Yagishita: Proc. SPIE **3150** (1997) 58.
13) M. Umeda, Y. Tezuka, S. Shin and A. Yagishita: Phys. Rev. B **53** (1996) 1783.
14) R. W. G. Wyckoff: *Crystal Structures* (Wiley Interscience, New York, 1964–71) 2nd ed., Vol. 1–6.
15) A. F. Wells: *Structural Inorganic Chemistry* (Clarendon Press Oxford, Oxford University Press, Oxford, 1984) 5th ed.
16) L. F. Mattheiss: Phys. Rev. B **5** (1972) 290.
17) L. F. Mattheiss: Phys. Rev. B **5** (1972) 306.
18) O. Gunnarsson and O. Jepsen: Phys. Rev. B **38** (1988) 3568.
19) K. Karlsson, O. Gunnarsson and O. Jepsen: J. Phys.: Condens. Matter **4** (1992) 2801.
20) K. Okada and A. Kotani: J. Electron Spectrosc. Relat. Phenom. **71** (1995) R1.
21) M. Nakazawa, S. Tanaka, T. Uozumi and A. Kotani: J. Phys. Soc. Jpn. **65** (1996) 2303.
22) D. K. G. de Boer, C. Haas and G. A. Sawatzky: Phys. Rev. B **29** (1984) 4401.
23) T. Idé and A. Kotani: J. Phys. Soc. Jpn. **67** (1998) 3621.
24) J. Zaanen, C. Westra and G. A. Sawatzky: Phys. Rev. B **33** (1986) 8060.
25) J. Park, S. Ryu, M. sup Han and S.-J. Oh: Phys. Rev. B **37** (1988) 10867.
26) K. Okada and A. Kotani: J. Phys. Soc. Jpn. **61** (1992) 4619.